Supplement of Atmos. Chem. Phys., 20, 8727–8736, 2020
https://doi.org/10.5194/acp-20-8727-2020-supplement

Atmospheric Chemistry and Physics
Open Access
EGU

Supplement of

Why is the Indo-Gangetic Plain the region with the largest NH_3 column in the globe during pre-monsoon and monsoon seasons?

Tiantian Wang et al.

Correspondence to: Yu Song (songyu@pku.edu.cn)

Contents of this file

Figures S1 to S5
Tables S1 to S2

Introduction

This supporting information consists of the following parts. Figure S1 shows spatial distributions of the emission fluxes of NH_3, SO_2 and NO_x over East Asia from June to August 2010 estimated using MIX database. Figure S2 shows the spatial distributions of SO_2 and NO_2 columns over East Asia. Figure S3 provides the comparation of the simulated SO_4^{2-} and NO_3^- concentrations in the base case and the increased emissions case. Figure S4 shows the spatial distribution of the NH_3 total columns from June to August 2010 derived from IASI measurements. Figure S5 shows spatial distributions of WRF-Chem predicted relative humidity and precipitation from June to August 2010, and the circles in Figure S5a represent the observed relative humidity obtained from NCDC dataset. Table S1 lists the options of WRF-Chem configurations. Table S2 provides the performance statistics of meteorological predictions of WRF-Chem.

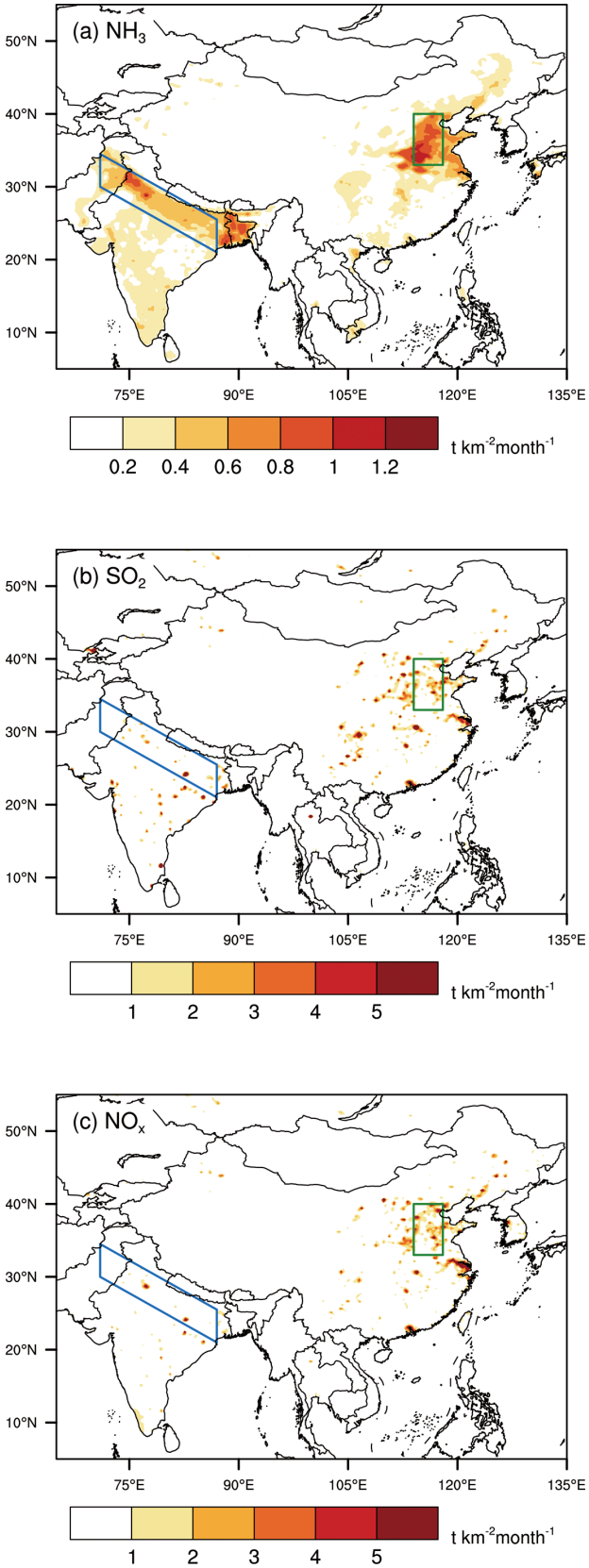

Figure S1. Spatial distributions of emission fluxes of (a) NH_3, (b) SO_2, and (c) NO_x over East Asia from June to August 2010. The blue quadrangle represents the IGP, and the green quadrangle represents the NCP.

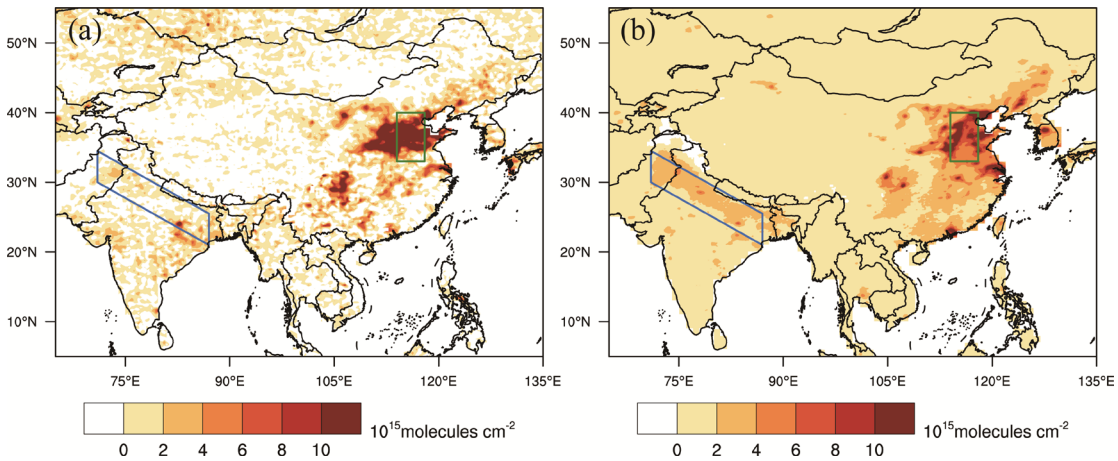

Figure S2. The spatial distributions of (a) SO_2 and (b) NO_2 columns over East Asia from June to August 2010.

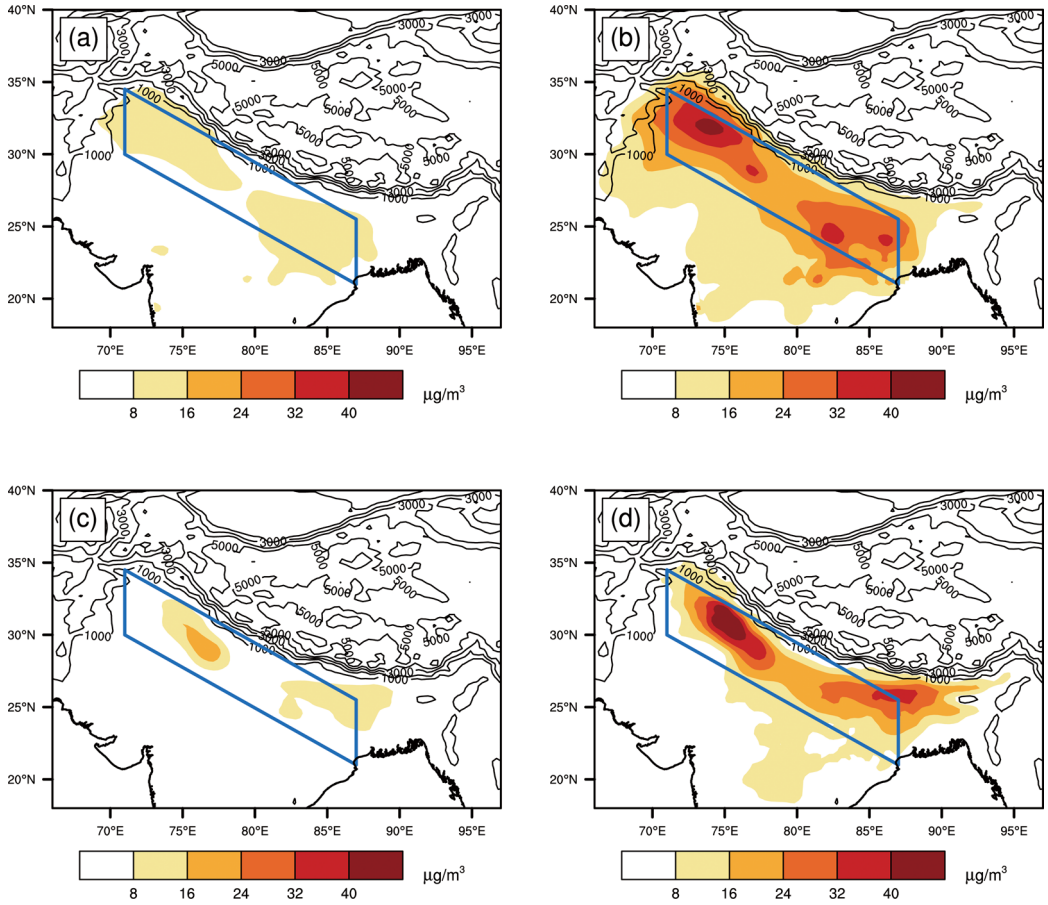

Figure S3. Spatial distributions of WRF-Chem predicted SO_4^{2-} and NO_3^- concentrations from June to August 2010. (a) and (b) are SO_4^{2-} concentrations in the base case and the increased emissions case, respectively. (c) and (d) are NO_3^- concentrations in the base case and the increased emissions case, respectively.

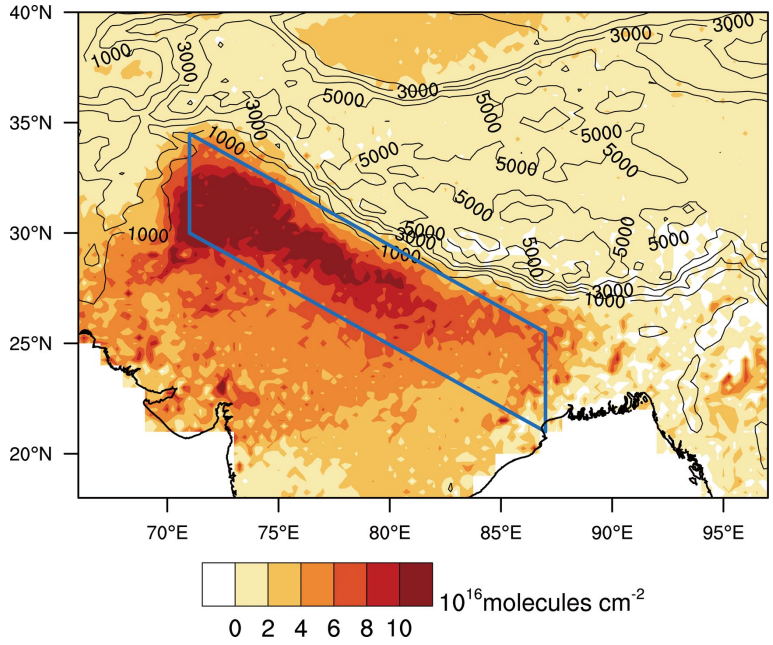

Figure S4. The spatial distribution of NH_3 total columns from June to August 2010 retrieved from IASI measurements.

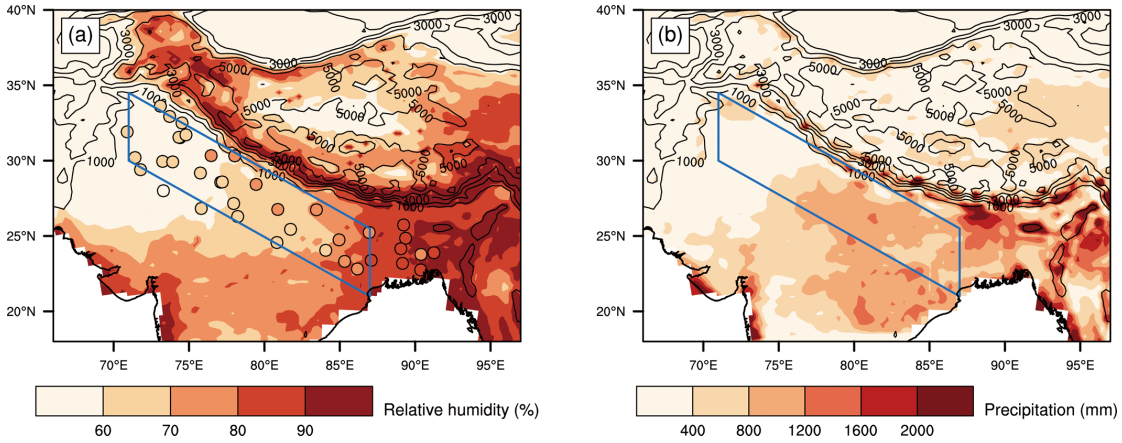

Figure S5. Spatial distributions of WRF-Chem predicted meteorological variables from June to August 2010. (a) Relative humidity. (b) Precipitation. Circles in (a) show the observed Relative humidity.

Table S1. WRF-Chem configurations

Meteorology initial and boundary conditions	Reanalysis data from the National Centers for Environmental Prediction Final Analysis (NCEP-FNL)
Shortwave radiation	rapid radiative transfer model (RRTMG)
Longwave radiation	rapid radiative transfer model (RRTMG)
Land surface model	Noah land-surface model
Planetary boundary layer model	Mellor-Yamada-Janjic (Eta) TKE scheme
Cumulus parameterization	New Grell scheme (G3)
Microphysics	Lin et al. Scheme
Photolysis	Fast-J photolysis

Table S2. Performance statistics of meteorological predictions of WRF-Chem.

	T2[a]	RH2[a]	WS10[a]	WD10[a]
Data pairs[b]	27508	27443	18036	18036
MeanObs[b]	30.9	69.3	2.7	165.1
MeanSim[b]	31.9	63.3	2.9	152.9
R[b]	0.8	0.8	0.1	0.4
MB[b]	0.9	-5.9	0.2	-12.1
RMSE[b]	3.6	19.8	2.7	95.2
NMB (%)[b]	3.0	-8.6	9.1	-7.4

[a] T2: temperature at 2 m; RH2: relative humidity at 2 m; WS10: wind speed at 10 m; WD10: wind direction at 10 m; SLP: sea level pressure.

[b] data pairs: the number of observed and simulated data pairs; MeanObs: mean observational data; MeanSim: mean simulation results; R: correlation coefficient; MB: mean bias; RMSE: root mean square error; NMB: normalized mean bias.